LANGMUIR

Article

pubs.acs.org/Langmuir

# Single-Molecule Peptide–Lipid Affinity Assay Reveals Interplay between Solution Structure and Partitioning

Tina R. Matin,[†] Krishna P. Sigdel,[†] Milica Utjesanovic,[†] Brendan P. Marsh,[†] Fabio Gallazzi,[‡] Virginia F. Smith,[§] Ioan Kosztin,[†] and Gavin M. King*[,†,∥]

[†]Department of Physics and Astronomy, [‡]Structural Biology Core, and [∥]Department of Biochemistry, University of Missouri-Columbia, Columbia, Missouri 65211, United States

[§]Department of Chemistry, United States Naval Academy, Annapolis, Maryland 21402, United States

Supporting Information

**ABSTRACT:** Interactions between short protein segments and phospholipid bilayers dictate fundamental aspects of cellular activity and have important applications in biotechnology. Yet, the lack of a suitable methodology for directly probing these interactions has hindered the mechanistic understanding. We developed a precision atomic force microscopy-based single-molecule force spectroscopy assay and probed partitioning into lipid bilayers by measuring the mechanical force experienced by a peptide. Protein segments were constructed from the peripheral membrane protein SecA, a key ATPase in bacterial secretion. We focused on the first 10 amino-terminal residues of SecA (SecA2-11) that are lipophilic. In addition to the core SecA2-11 sequence, constructs with nearly identical chemical composition but with differing geometry were used: two copies of SecA2-11 linked in series and two copies SecA2-11 linked in parallel. Lipid bilayer partitioning interactions of peptides with differing structures were distinguished. To model the energetic landscape, a theory of diffusive barrier crossing was extended to incorporate a superposition of potential barriers with variable weights. Analysis revealed two dissociation pathways for the core SecA2-11 sequence with well-separated intrinsic dissociation rates. Molecular dynamics simulations showed that the three peptides had significant conformational differences in solution that correlated well with the measured variations in the propensity to partition into the bilayer. The methodology is generalizable and can be applied to other peptide and lipid species.

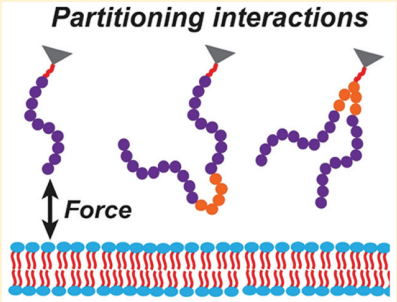


## INTRODUCTION

Protein–lipid interactions are fundamental in biology. These interactions directly affect the activity of peripheral membrane proteins as well as the three-dimensional shape and function of integral membrane proteins.[1−3] Such interactions also govern the action of antimicrobial peptides and have been exploited for the delivery of therapeutic agents through the development of cell-penetrating peptides.[4,5] Probing these interactions via macroscopic measurements can yield highly informative quantities such as the solution-to-bilayer transfer free energy, but mechanistic details are obscured by asynchronous activities inherent in the partitioning process.[6] Further, lipophilic peptides often aggregate, complicating the monomeric partitioning results. Thus, despite broad significance, peptide–lipid interactions have proven difficult to study and, consequently, remain poorly understood. This is largely due to the lack of a suitable methodology that is capable of quantitatively probing the interaction of lipophilic polypeptide chains with membrane interfaces in physiological conditions.

Atomic force microscope (AFM)-based single-molecule force spectroscopy is a powerful established technique that is frequently used to reveal the unfolding pathways of multimeric integral membrane proteins such as bacteriorhodopsin.[7−9] When performing AFM-based force spectroscopy experiments, it is common to discard rupture events that occur very close to the sample surface and to consider them nonspecific.[7,10] However, this is precisely the data that capture peptide–lipid interactions. This highlights the need for sub-pN force measurements that can resolve interactions occurring at a single planar interface. By contrast, conventional AFMs have force precision around 10 pN.[11] Using stacked lipid bilayers may circumvent the single planar interface requirement,[12] but controlling the number of bilayers in a stack is difficult and peptide insertion across more than a single bilayer is not possible, in general. Additionally, utilizing concatenated peptide constructs, as we demonstrate here, is also feasible, but peptide–peptide interactions can then conceal the desired monomeric peptide–lipid bilayer interaction. Most membrane protein studies have focused on two-dimensional protein arrays,[8] the close-packed nature of which significantly suppresses the diffusion in the membrane; proteins embedded in bicelles are a notable exception.[13] A handful of groups[14−20] have probed protein–lipid interactions using bilayers that maintain significant lipid mobility even when in close proximity to surfaces,[21] but the lack of precision of the force measurements (≥10 pN) has hampered the interpretation.

**Received:** January 12, 2017
**Revised:** March 2, 2017
**Published:** March 27, 2017





DOI: 10.1021/acs.langmuir.7b00100
*Langmuir* 2017, 33, 4057−4065

Our group has taken a two-pronged approach to demonstrate a robust and precise peptide−lipid bilayer interaction assay. In one line of inquiry,[22] the chemical composition of a peptide was altered while holding its geometry constant; single amino acid changes were distinguished. In a second line of inquiry—the work described here—the geometry of a peptide was varied while its chemical composition was kept (nearly) constant. To this end, we developed a precision single-molecule assay to probe the interactions between proteins based on SecA and a model single component lipid bilayer, 1-palmitoyl-2-oleoyl-*sn*-glycero-3-phosphocholine (POPC).

Peripheral membrane protein SecA and the integral translocon (SecYEG) are essential components of the general secretory system, which constitutes the major route of protein export from the cytosol of all eubacteria.[23] Since its original identification,[24] ATPase SecA has been known to be distributed between the cytosol and the membrane.[25,26] Our group and others have shown that SecA−lipid interactions are fundamental to the operation of the general secretory system and that the extreme amino-terminal region of SecA is a locus for the interaction with the membrane.[27−30] In particular, deletions of the first 10 amino acids of SecA result in a significant reduction in translocation of precursor proteins across the membrane.[29] Inspired by the significant impact a peptide−lipid bilayer interaction can have on the function of the general secretory system, we sought to explore the nature of this interaction from a mechanical, single-molecule perspective.

We investigated the interaction between the first 10 amino-terminal residues of SecA (SecA2-11) and supported POPC bilayers using AFM-based force spectroscopy with sub-pN precision.[11] To guide the interpretation, three peptide geometries were studied: single copy SecA2-11, two copies of SecA2-11 linked in series, and two copies of SecA2-11 connected in parallel. The three constructs exhibited distinct signatures in force spectra and significant differences in membrane activity (i.e., the probability of partitioning into the membrane). Energetic landscape modeling revealed multiple distinct dissociation pathways that varied with the peptide geometry. Further, partitioning measurements were corroborated with solution structures, as determined via molecular dynamics (MD) simulations. Taken together, our work engenders confidence in a single-molecule peptide−lipid bilayer affinity assay and provides novel characterization of a peptide−lipid interaction related to the activity of an important peripheral membrane protein.

## RESULTS AND DISCUSSION

An overview of the experimental approach (Figure 1) shows three different peptide geometries tethered to AFM tips for force spectroscopy experiments. Peptides were synthesized with a C-terminal cysteine (Figure 1, green; see Materials and Methods for details), enabling site-specific covalent linkage to the AFM tip through a ∼9.5 nm long flexible hydrophilic linker [24 ethylene oxide (PEG) subunits].[31] The linker minimizes interactions with the surface of the AFM tip while allowing multiple binding orientations in the bilayer. The dimeric constructs, which were 96% identical in amino acid (aa) content, had short 5 aa glycine-rich internal linkers to provide conformational freedom between the repeated SecA2-11 sequences (Figure 1b,c, orange). Tip functionalization conditions were optimized at low concentration to yield approximately one peptide tethered near the tip apex (section S1). Supported lipid bilayers, robust mimics of the biological membrane,[32−34] were formed on a cleaned microscope cover glass using established techniques.[35,36]

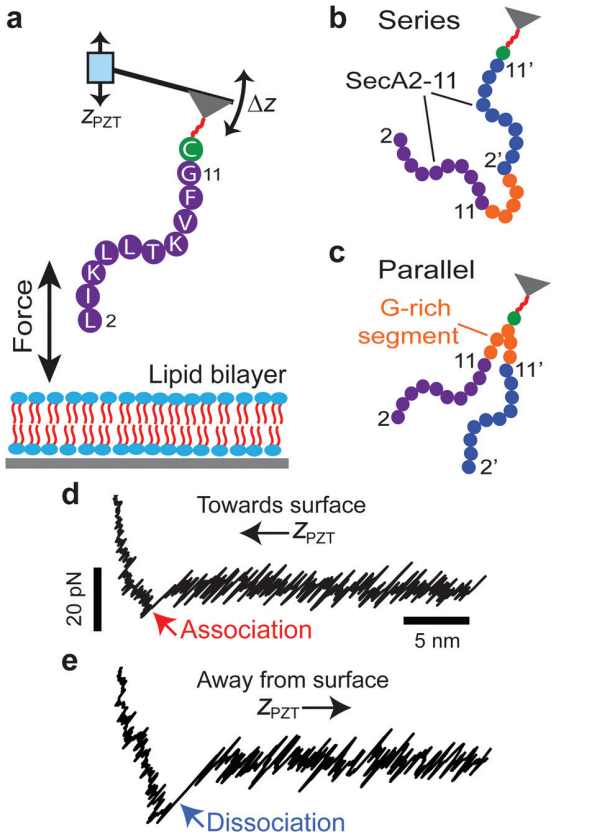


**Figure 1.** Mechanical protein−lipid interaction assay. (a) Single copy SecA2-11 (purple) covalently affixed to the AFM tip through a flexible PEG linker (red, not to scale). The piezoelectric (PZT) stage affixed to the base of the cantilever is translated vertically $z_{PZT}$, whereas the interaction force transmitted to the cantilever is recorded through the deflection observable, $\Delta z$. Sketches of (b) two copies of SecA2-11 linked in series and (c) two copies of SecA2-11 linked in parallel. Dual-copy sequences were separated by glycine-rich segments (orange); primed notation (2′-11′, blue) identifies the copy nearest the tip for the series construct and the isopeptide-bonded branch for the parallel construct. (d) Approach data exhibiting an association event (red arrow). Retraction curve (e) showing a dissociation event (blue arrow). (d,e) Force is plotted vs height of the tip apex above the bilayer ($z_{PZT} - \Delta z$), data for single copy SecA2-11, $\left|\frac{dz_{PZT}}{dt}\right| = 100$ nm/s.

The cantilever underwent a cyclical trajectory in the experiments. Peptide-functionalized tips were first advanced toward the lipid bilayer. In about 20% of the attempts, an association event was observed as the tip approaches the bilayer. Upon contact with the membrane (compressive force threshold ∼100 pN), the tip advance was halted for 1 s. Then, the direction of the piezoelectric stage affixed to the base of the cantilever ($z_{PZT}$) was reversed. Dissociation (rupture) events occurred frequently (in >50% of attempts) during retraction. Both association and dissociation events were defined by sudden, larger than 5 pN, changes in force. We note that this assignment would not be possible using conventional AFMs with ∼10 pN force precision. Figure 1d,e illustrates association and dissociation events for single copy SecA2-11 interacting with a POPC bilayer. We hypothesized that chemically similar,


DOI: 10.1021/acs.langmuir.7b00100
*Langmuir* 2017, 33, 4057−4065

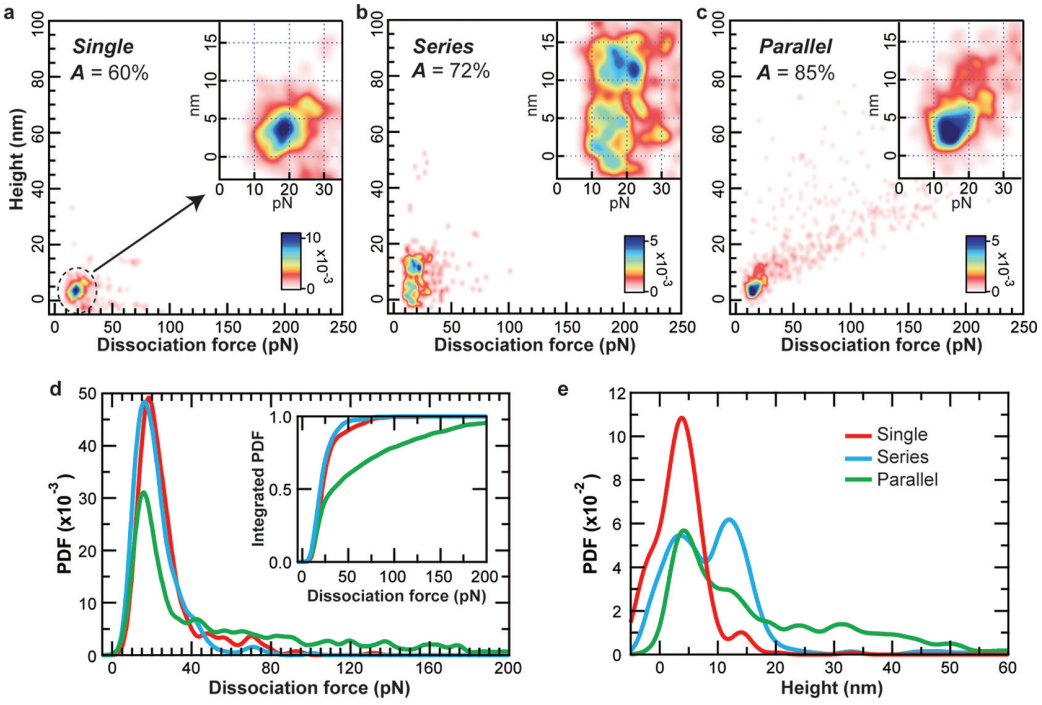


**Figure 2.** Dissociation data correlate with the peptide geometry. (a) Two-dimensional probability density map of dissociation force and corresponding height of the tip apex above the bilayer at which the dissociation event occurred for single copy SecA2-11 and POPC ($N_e$ = 303, $N_t$ = 5, activity ≡ $A = N_e/N_a \times 100\%$). Data for the (b) series ($N_e$ = 357, $N_t$ = 5) and (c) parallel ($N_e$ = 667, $N_t$ = 8) constructs. (d) One-dimensional probability density functions (PDF) compare the force distributions for each construct (*single copy*, red; *series*, blue; and *parallel*, green). Inset: integrated PDFs indicate that >90% of events occur at forces <50 pN for single copy and series. (e) Positional PDF showing all constructs. Note the prominent bimodal nature of the series construct.

yet geometrically different, peptides would produce distinguishable interaction signatures with membranes.

**Expected Correlations between Peptide Geometry and Force Spectra were Observed.** We carried out experiments to verify that specific changes in peptide geometry unequivocally alter the interaction patterns with model lipid bilayers. Tips were prepared with single copy, series, or parallel peptide constructs and allowed to interact with POPC. Force curves were analyzed to yield ordered pairs for each dissociation event, representing the rupture force magnitude and the corresponding height of the tip apex above the lipid bilayer at which the dissociation event occurred. Interaction maps resulting from this analysis (Figure 2a, single copy; b, series; and c, parallel) show significant differences. Activity, $A$, is defined as the number of events, $N_e$, divided by the number of attempts, $N_a$, expressed as a percentage. $N_t$ is the number of tips in the analysis. Control experiments showed that the great majority (>97%) of dissociation events can be attributed to specific peptide−lipid interactions (section S2). Moreover, artifacts where lipid remains adhered to the AFM tip for multiple force−distance curves[18] were not observed for the core SecA2-11 construct (section S3).

Both the series and parallel constructs exhibited a population of rupture events at approximately the same location in force−position space as the single-copy peptide (18.6 ± 4.8 pN, 3.8 ± 3.3 nm, mean ± standard deviation). We emphasize that this was the only prominent population observed for the monomeric construct. By contrast, the dimeric series construct exhibited a bimodal position−space distribution with a second and more pronounced population centered at similar force (~18 pN) but at a higher position above the bilayer (11.9 ± 4.6 nm, Figure 2e, blue). The contour length of the series construct including the PEG linker is 19.9 nm (assuming 0.4 nm per residue[37]); the stochastic vertical offset between the absolute tip apex and the linker attachment point leads to uncertainties in measured molecular extension.[38] MD simulations of the series construct (discussed below) suggest that the population of events at the lower position (~3.8 nm) is likely due to a compact conformation of this dimeric peptide.

The parallel construct, in contrast to both single copy and series, exhibited a long tail of rupture events extending well beyond 50 pN. This tail contained a significant fraction of the total population (40%, Figure 2d, inset) and appeared likely to be associated with pulling of lipid molecules from the bilayer surface.[39,40] Indeed, control experiments using bilayers rigidified with photopolymerized tail groups provided evidence that this was likely occurring with the parallel peptide (section S4).

Though all three peptides exhibited a dissociation population at around 20 pN, indicative of a common last rupture mode of the core SecA2-11 monomer, significant differences were observed that correlated with the peptide length and topology (number of endpoints). One may intuitively expect that higher dissociation forces would be required for the dimer constructs because the number of hydrophobic residues is twice that of the monomer. However, the observed interaction behavior of the dimeric constructs was not additive. Rather, the data indicate that intrapeptide interactions occurring within the series and parallel constructs produce a richer behavior, for example, causing the parallel dimer to be more lipid-active than the series. To summarize, prominent signatures in the force spectra



DOI: 10.1021/acs.langmuir.7b00100
*Langmuir* 2017, 33, 4057−4065

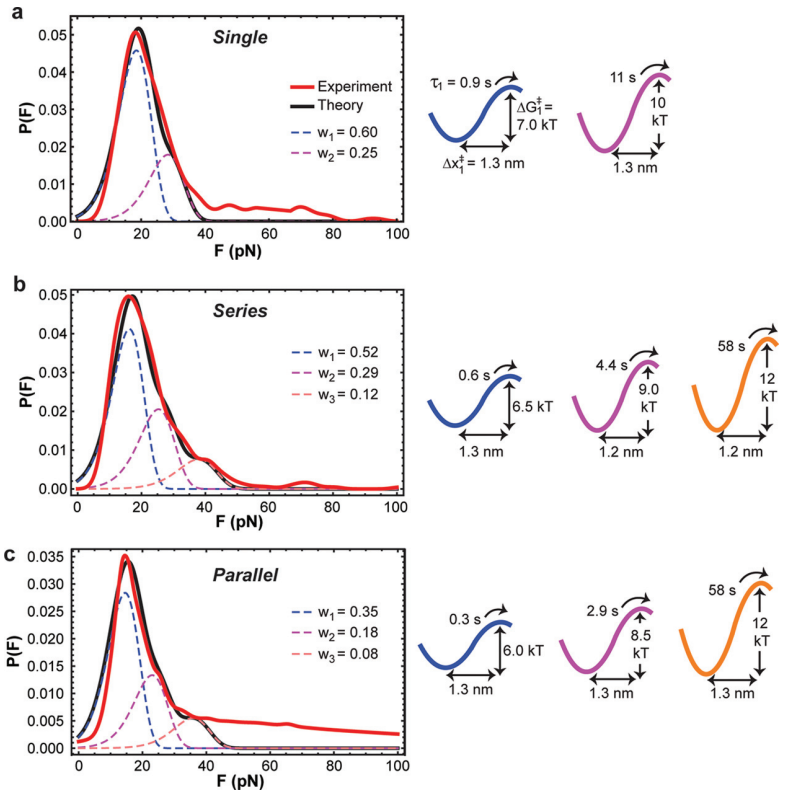


**Figure 3.** Energetic landscapes vary with the peptide geometry. (a) Rupture force distribution $P(F)$ for SecA2-11 single copy and POPC required two model force distributions (dashed) corresponding to two prominent dissociation pathways, occurring with probabilities $w_1$ and $w_2$. These pathways have distinct potential barriers (color coded as in dashed) and well-separated dissociation rates ($1/\tau_i$). Changing peptide geometry to (b) series and (c) parallel altered the first two barriers slightly and opened an additional low-probability, high-barrier pathway at $12kT$. Weighting factors sum to <1 because a minimal number of model distributions were used to capture the main peaks (>60%) of the experimental distributions.

mapped to specific peptide geometries; these results engender confidence in the assay and in its quantitative interpretation.

**Characterizing the Energy Landscape of a Peptide–Lipid Interaction.** Single-molecule unfolding experiments typically involve breaking specific bonds that stabilize the macromolecule (e.g., titin, RNA hairpins, and bacteriorhodopsin). The rupture force distributions, $P(F)$, resulting from these measurements usually have a simple (albeit asymmetric) bell curve shape.[41−43] The situation is more complex for a peptide dissociating from a fluid lipid bilayer, due, in part, to the multiplicity of binding orientations that may occur. For example, long-timescale MD simulations of similar peptide–lipid systems show positional and rotational subpopulations at equilibrium.[22]

To account for complex peptide–lipid interaction topography, we extended a theoretical model[41,42] relating $P(F)$ to the intrinsic kinetics of molecular rupture events that take place along multiple pathways, instead of a single one. Assuming that rupture events along the $i^{\text{th}}$ pathway occur with probability $w_i$, one can write $P(F) = \sum_{i=1}^{N} w_i P_i(F)$. The individual rupture force distributions, $P_i(F)$, can be expressed in terms of the force-loading rate, $\dot{F} = dF/dt$, and the corresponding force-dependent rupture rates $k_i(F)$ (see Materials and Methods). On the other hand, the individual rupture rates can also be expressed in terms of the corresponding (i) free-energy barrier height, $\Delta G_i^{\ddagger}$; (ii) distance between the bound and transition states, $\Delta x_i^{\ddagger}$; and (iii) intrinsic rupture rate in the absence of the pulling force, $k_{0i} = k_i(0)$. Thus, to quantitatively characterize peptide–lipid interactions, one needs to determine $\Delta G_i^{\ddagger}$, $\Delta x_i^{\ddagger}$, and $k_{0i}$ for the dominant pathways, with the highest statistical weights $w_i$, by fitting the experimentally measured $P(F)$ using the theoretical model.

**Kinetic Pathways Depend on Peptide Geometry.** Analysis of the rupture force distribution for single copy SecA2-11 interacting with POPC revealed that there are two prominent dissociation pathways at a pulling speed of $v$ = 100 nm/s (Figure 3a). The first pathway, with free-energy barrier $\Delta G_1^{\ddagger} = 7kT$, occurs with a probability $w_1$ = 60% and an intrinsic dissociation rate of $k_{01}$ = 1.1 $s^{-1}$. The second pathway has a larger barrier, $\Delta G_2^{\ddagger} = 10kT$, a smaller intrinsic dissociation rate, $k_{02}$ = 0.09 $s^{-1}$, and occurs with a lower probability $w_2$ = 25%. These two pathways account for the majority (85%) but not all of $P(F)$. The difference corresponds to the difficult-to-sample large force tail of $P(F)$ and can be accounted for by pathways with higher $\Delta G_i^{\ddagger}$ ($i > 2$), which occur less frequently. Additionally, because the statistical weight of each dissociation pathway is known, one can deduce an aggregate escape time $\tau = \sum_i w_i \tau_i$ and hence an effective off-rate $k_{\text{off}} = \frac{1}{\sum_i w_i \tau_i}$. This analysis yields $k_{\text{off}}$ = 0.3 $s^{-1}$ for the SecA2-11 single-copy construct and POPC.

Analysis of the series and the parallel constructs revealed three kinetic barriers (Figure 3b,c). The first two barriers for both of these repeated constructs were slightly lowered (reduced by ~$1kT$) compared with the single-copy construct. The difference, as illustrated in MD simulations (Figure 5), is likely due to the prevalence of intrapeptide interactions



DOI: 10.1021/acs.langmuir.7b00100
Langmuir 2017, 33, 4057−4065

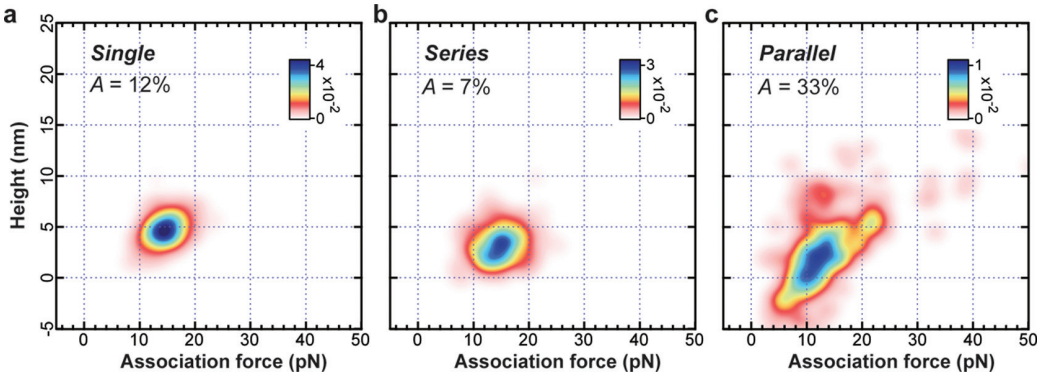


**Figure 4.** Association interactions vary with peptide geometry. (a) Two-dimensional probability distributions showing association events as the tip approaches for single copy SecA2-11 ($N_e$ = 261, $N_t$ = 8). Data for series ($N_e$ = 205, $N_t$ = 9) and parallel ($N_e$ = 217, $N_t$ = 8) constructs are shown in (b) and (c), respectively. Activities, $A$, show the association propensity for the parallel construct was 4.7-fold higher compared with the series peptide.

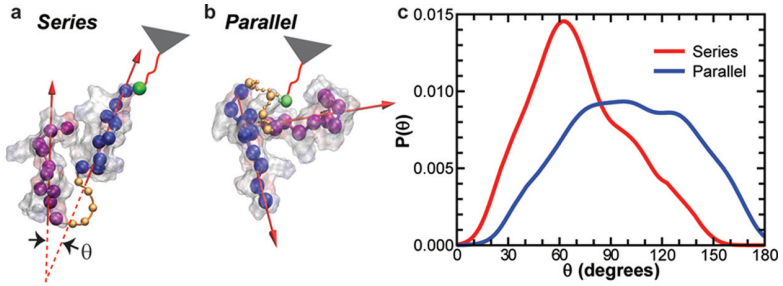


| | Residue | Radius of gyration [Å] | H-bonding [% occupied] | | Leu accessibility to solvent [Å$^2$] | $\theta$ [deg] |
|---|---|---|---|---|---|---|
| Single | 2-11 | 6.7 ± 0.8 | L5 ··· T7 | 4% | 490 ± 31 | |
| Series | 2-11 | 6.9 ± 0.4 | K8′ ··· L2 | 21% | 379 ± 44 | 72 ± 29 |
| | | | L2 ··· T7 | 5% | | |
| | | | L5 ··· V9 | 4% | | |
| | 2′-11′ | 6.6 ± 0.8 | T7 ··· L2 | 1% | 396 ± 78 | |
| | All | 9.9 ± 1.7 | 31% | | 775 ± 105 | |
| Parallel | 2-11 | 7.3 ± 0.9 | K8′ ··· G11 | 20% | 501 ± 46 | 101 ± 35 |
| | | | K8′ ··· G13 | 18% | | |
| | | | L5′ ··· G13 | 13% | | |
| | 2′-11′ | 6.8 ± 0.5 | T7 ··· I3 | 11% | 480 ± 38 | |
| | All | 12.0± 2.2 | 62% | | 981 ± 60 | |

**Figure 5.** Peptide solution structure via MD simulations. Snapshots of (a) series and (b) parallel constructs in solution at room temperature (water has been removed for clarity). Unprimed residues are drawn purple, primed blue (as defined in Figure 1). The orientation of the repeated peptide sequences was characterized by the angle $\theta$ between the axes (red arrows) of the peptides. (c) Comparison between the probability distributions $P(\theta)$ for the two constructs indicating that the parallel construct is more open, in general, whereas the series is more compact and folded upon itself. Table: parameters calculated from the MD simulations. For series and parallel constructs, quantities were calculated for each copy of SecA2-11, as well as for the complete peptide.

competing with the bilayer in the dimeric constructs. We note that the high force tail (>50 pN) in $P(F)$ for the parallel peptide is not included in the modeling.

Our analysis shows that a relatively simple peptide−lipid interaction (10 amino acids, single component lipid bilayer) can exhibit $N > 1$ distinct dissociation pathways. Further, the nature of the potential barriers varies with the peptide geometry. Therefore, it seems possible that other factors could influence the interaction. Secondary structure can emerge when a peptide binds to the lipid bilayer.[3] We performed circular dichroism (CD) measurements to quantify this effect (section S5). CD results indicate that the core SecA2-11 sequence remains predominantly unstructured when in solution (in agreement with MD simulations), as well as when in the presence of POPC liposomes (maximum of ∼15% helix at 1 mM lipid). Hence, the secondary structure effects are negligible in this system, and the observed dynamics are driven by the primary structure of the peptide.

**Association Probability Varies with the Peptide Geometry.** Acquiring data while the peptide-decorated tip approaches the bilayer surface provides a direct observation of partitioning into the membrane. The three geometrically distinct constructs exhibited a single prominent mode when associating with POPC bilayers. Both the single copy and series constructs had a nearly identical mean partitioning force magnitude (15 pN, Figure 4a,b). The distribution for the



DOI: 10.1021/acs.langmuir.7b00100
Langmuir 2017, 33, 4057−4065

parallel construct was more diffuse (Figure 4c), exhibiting a majority population centered at ∼12 pN and a small subpopulation (<10% of total) at approximately twice this value.

A pronounced difference in the partitioning was evident in the membrane activity. In particular, for the series construct, only 7% of approach curves (out of $N_a$ = 2800) exhibited a partitioning event. By contrast, the parallel construct was 4.7-fold more active ($A$ = 33%). The association activity of the single-copy construct was found to be intermediate between the series and parallel constructs ($A$ = 12%, 2200 attempts).

Therefore, the data suggest that the peptide solution structure is directly influencing the partitioning activity as the tip approaches the bilayer. The 4.7-fold increase in association probability of the parallel over the series construct is surprising because the chemical content of both peptides is nearly identical (25 out of 26 aa) as is the lipid species (POPC). Further, the activity for the same two peptides when dissociating from the membrane was nearly the same (1.2-fold enhancement for the parallel peptide, Figure 2). This serves as an important control, ruling out the significant differences in peptide-tethering density.

**Peptide Solution Structure Correlates with Association Probability.** Intrapeptide interactions between repeated SecA2-11 sequences in the series and parallel constructs could compete with the lipid bilayer and give rise to differences in the association activity. We performed MD simulations to evaluate these effects and to correlate the structural information with the experimental findings. The results show (Figure 5, see Materials and Methods for details) that the individual SecA2-11 peptides have a compact coil structure in solution, as indicated by the small values of the radius of gyration, $R_g$. At the same time, the mean radius of gyration, $\langle R_g \rangle$, for the entire repeated constructs was >20% larger in the parallel case compared with the series. Thus, the series is significantly more compact than the parallel, as a result of the differences in the relative orientation of the repeated sequences in the two systems.

To further quantify the conformational differences between the two dimeric constructs, we followed the time evolution and statistics of the angle $\theta$ between the axes of the two peptides (Figure 5a−c). The peak position in the distribution function $P(\theta)$ for the series construct is considerably smaller than that for the parallel, indicating that the two SecA2-11 monomers in the series system tend to attract each other, whereas, in the parallel case, they repel. Hence, the series forms a more compact structure than the parallel, in agreement with the $R_g$ results. The dominant orientation for the parallel peptide is splayed outward (Figure 5b), with a ∼100° angle between the repeated SecA2-11 sequences, stabilized by hydrogen bonding. With both N-termini available, this splayed geometry is poised to interact with the bilayer surface significantly more than the compacted series construct (Figure 5a). Additional factors are likely contributing to the observed variations in the membrane activity.

To a great extent, the membrane affinity of SecA2-11 is likely due to the hydrophobic leucine residues located at the extreme N-terminus and at positions 5 and 6. Taken together, these three residues constitute 30% of the core SecA2-11 sequence. Hence, we evaluated the freely accessible surface area[44] of this lipophilic residue. The results showed a >25% enhancement in the accessibility of leucine for the parallel construct compared with the series. Therefore, factors including a less compact, splayed orientation, and greater accessibility of hydrophobic residues impart significant advantages upon the parallel construct for partitioning when compared with the series construct. To summarize, MD simulations revealed that both the series and parallel constructs interacted strongly with themselves; however, the consequences of the intrapeptide interactions on the conformations were distinct and provide a molecular-level justification for the experimental observations.

## CONCLUSIONS

We demonstrated that a single-molecule peptide−lipid interaction assay can be robust, precise, and interpretable. Distinct signatures in measured force spectra mapped directly to the specific changes in peptide geometry. To extract energetic landscape information amid the topographical complexity inherent in peptide−lipid interactions, the dissociation process was modeled as an escape of an overdamped stochastic particle from coexisting potential wells with varying weights. The energy landscapes that emerged were complex. Analysis revealed multiple partitioning pathways with distinct probabilities as well as off-rates in the absence of force that varied with the peptide geometry. Even the single-copy peptide, which is short and unstructured, exhibited two main dissociation pathways from the single component lipid bilayer. Although peptide−lipid interactions are often described in terms of electrostatic interactions, hydrophobicity, and secondary structure formation, our CD measurements suggested that the secondary structure is minimal for SecA2-11 in contact with POPC. Other factors may also be involved, including lipid bilayer perturbations. Further work will be required to deconvolve specific contributions to the kinetic pathways.

Using series and parallel peptides with different geometries, but near identical chemical composition, provided a means to isolate the role of the peptide structure in partitioning. MD simulations revealed solution structures that would clearly modify the membrane activity and do so in a manner consistent with the experimental results, which showed an approximately 5-fold enhancement in bilayer association probability for the parallel peptide compared with the series. In summary, we united high-precision single-molecule methods with analytical modeling, computational simulations, and bulk biochemical techniques and thus characterized a peptide−lipid bilayer interaction related to the mode of action of a model peripheral membrane protein. More generally, our work provides a framework to advance the understanding of other protein−lipid interactions, including with biologically relevant lipid mixtures.

## MATERIALS AND METHODS

**Peptide Synthesis.** Peptides were synthesized in a model 396 multiple peptide synthesizer (AAPPTec, Louisville, KY) using solid-phase synthesis on Sieber amide resin and standard Fmoc/*t*Bu chemistry for linear elongation, resulting in purities >95%. Three geometrically distinct constructs were made: single copy SecA2-11, LIKLLTKVFG-C; series, LIKLLTKVFG-GGSGG-LIKLLTKVFG-C; and parallel, 2 × [LIKLLTKVFG-GG]-K-C. The parallel construct was synthesized using a multiple antigenic peptide approach. For this peptide, an in-house optimized protocol was used to reduce the substitution level of the resin.[45] This was achieved by undercoupling the resin with the first protected aa for an extended period of time and subsequently capping the unreacted amino groups still on the resin with acetic anhydride. Cleavage and side chain deprotection were achieved by treating the peptidyl-resin with 85% trifluoroacetic acid and scavengers (ethanedithiol, thioanisole, phenol, water, and triisopropylsilane, 2.5% each). The obtained crude product was



DOI: 10.1021/acs.langmuir.7b00100
*Langmuir* 2017, 33, 4057−4065

characterized using high-performance liquid chromatography (HPLC, Beckman Coulter) and mass spectroscopy (MS, Thermo Fisher Scientific, section S6), purified by MS-assisted semipreparative HPLC using an in-house optimized multistep gradient, and finally recovered using lyophilization.

**Lipid Bilayer Preparation.** Liposomes were prepared by extrusion of POPC (Avanti) suspended in 50 mM sodium phosphate pH 7.2, 50 mM NaCl, and 10 mM ethylenediaminetetraacetic acid through a membrane (approximately 25 times) with a 100 nm pore diameter. Supported bilayers were formed by vesicle fusion (70 $\mu$M, 30 min incubation, ~30 °C) to clean glass surfaces,[35,36] which were rinsed (0.1 mL buffer solution, 3×) before force spectroscopy experiments. AFM imaging confirmed bilayer fusion and coverage (section S7). All experiments were performed at ~30 °C, well above the gel-to-fluid transition temperature of POPC (−2 °C).

**Tip Functionalization.** To enhance force precision, the metal coating on the tips (BioLever, BL-RC-150VB, Olympus, $k \approx 6$ pN/nm) was first removed using gold etchant and chromium etchant (Transene).[11] Tips were then functionalized following an established procedure using a PEG linker,[31,46] which allowed the peptides to orient freely and minimized the interactions with the surface of the AFM tip. Briefly, tips were plasma cleaned (10 min, 30 W, Harrick Plasma) and then immersed in silane (3-ethoxydimethylsilyl)-propylamine (Sigma Aldrich) for 60 s and baked at 80 °C for 30 min. These dry tips were incubated in borate buffer (50 mM $Na_2B_4O_7 \cdot 10H_2O$, pH 8.5) for 1 h, followed by NHS-$PEG_{24}$-maleimide (Thermo Scientific) solution for 1 h, and then in peptide solution for 2 h. Finally, the tips were washed (75 mM $Na_3PO_4$, pH 7.2) and loaded into the microscope for force spectroscopy experiments. Obtaining zero tethers on a tip apex was the most common failure mode (occurring in ~50% of preparations).

**Force Spectroscopy.** AFM experiments were performed in buffer solution (10 mM HEPES pH 7.6, 300 mM KAc, 5 mM $Mg(Ac)_2$) at ~30 °C using a commercial instrument (Cypher, Asylum Research). Force spectra were acquired in the force map mode. As expected for continuous lipid bilayers with minimal defects, the tip−sample interaction did not vary significantly over spatial areas varying between 500 × 500 nm$^2$ and 20 × 20 $\mu$m$^2$ (section S8). The stage affixed to the base of the cantilever controlled the cantilever speed (100 nm/s), resulting in an effective loading rate in the range of 400−700 pN/s. Spring constants were measured using the thermal method.[47] The hold time and compressive force applied to the surface between approach and retraction were held constant (1 s, ~100 pN).

**Data Analysis.** Partition and rupture events were characterized by two parameters: the magnitude of the abrupt change in force and the corresponding height of the tip apex above the lipid bilayer surface at which the abrupt force change occurred. In the cases (<20% of total) where multiple rupture events were observed in a single trace, we analyzed only the last rupture (i.e., the event occurring the furthest from the bilayer surface). The position where the events occurred was determined by the difference $z_{PZT} - \Delta z$, where $\Delta z$ is the cantilever deflection. The zero point in height was defined by the intersection between linear fits to the zero-force baseline and the steep linear slope that emerged when the tip was in contact with the lipid bilayer. Kernel density estimation with a bivariate Epanechnikov kernel was used to create the two-dimensional (force, height) density plots, which were volume normalized to unity.

**CD Spectroscopy.** CD spectroscopy was performed to evaluate the secondary structural content of the SecA2-11 peptide in solution and in contact with lipids. A JASCO J-815 spectrophotometer was used. Spectra were recorded from 190 to 260 nm using a 1 mm path length quartz cuvette in a thermostated sample compartment maintained at 8 °C. The step-size was 0.5 nm, the bandwidth was 1 nm, and the scan rate was 20 nm/min. The averaged spectra were smoothed using a five-point moving average algorithm. The peptide concentration was 45 $\mu$M, and the total lipid concentration varied between 0 and 1000 $\mu$M. Constant pH was maintained using 10 mM Tris, pH 7.6 buffer. All peptide−lipid titrations were performed in triplicate. Deconvolution of the averaged spectra was performed using the CDSSTR program[48] accessed through the DichroWeb online user platform.[49] The CDSSTR program deconvolutes a spectrum to provide estimated percentages of the alpha helix (regular and distorted), the beta strand (regular and distorted), turns, and the disordered content.

**Theoretical Modeling.** Molecular rupture induced by a gradually increasing force is usually modeled as an escape process of a Brownian particle over a single free-energy barrier.[41,42] As long as the force-loading rate, $\dot{F} = dF/dt$, is not too large, the rupture force distribution, $P(F)$, is related to the force-dependent dissociation (off) rate, $k(F)$, through $P(F)dF = -dS = k(F)S(t)dt$, where $S(F(t))$ is the rupture survival probability. However, when molecular rupture events can occur along several distinct pathways, as in the experiments described here, that involve different dominant free-energy barriers, the survival probability becomes a sum of exponentials and $P(F)\ dF = \sum_i w_i P_i(F)\ dF = -\sum_i dS_i = \sum_i k_i(F)S_i(t)\ dt$, where $w_i = S_i(0)$ is the probability that the process follows the $i$th pathway. Similar to the single barrier case, one finds $P(F) = \sum_i w_i P_i(F)$, with $P_i(F) = [k_i(F)/\dot{F}] \exp(-\int_0^F [k_i(f)/\dot{F}]df)$. Because $\sum_i w_i = 1$, one can verify that $P(F)$ is normalized to unity. The individual rupture rates can be calculated as the inverse mean first passage time (MFPT) from the bottom ($x_{i-}$) to the top ($x_{i+}$) of the free-energy profile, $U_i(x)$, in the presence of the pulling force, $k_i(F) = D_i / \int_{x_{i-}}^{x_{i+}} dy \exp[\beta U_i(y)] \int_{-\infty}^{y} dz \exp[-\beta U_i(z)]$. Here $U_i(x) = U_{i0}(x) - Fx$, where $U_{i0}(x)$ is the intrinsic free-energy landscape along the pulling direction, $D_i$ is the diffusion coefficient, and $\beta = 1/k_B T$, where $k_B$ is the Boltzmann's constant and $T$ is the absolute temperature. Note that, unlike the widely used Kramers formula for high barriers, the MFPT formula is valid for arbitrary barrier heights. It was shown that the free-energy surface $U_i(x)$ can be well-parametrized by the barrier height $\Delta G_i^{\ddagger}$ and the distance $\Delta x_i^{\ddagger} = x_{i+} - x_{i-}$ between the bound and transition states.[41,42] Thus, for constant force-loading rate, $k_i(F)$ and $P(F)$ depend only on the parameters $\Delta G_i^{\ddagger}$, $\Delta x_i^{\ddagger}$, and $D_i$ or, equivalently, the intrinsic escape time $\tau_i = 1/k_i(0)$. Of course, the shape of the measured $P(F)$ depends on the weights $w_i$, which differ from one experiment to another.

**MD Simulations.** *Building the Structures.* All atom models of the three SecA2-11 constructs (i.e., single copy, series, and parallel), including glycine-rich linkers, were built from the primary structures by using the Molefacture plugin in the VMD[50] molecular visualization and modeling software. Building the parallel SecA2-11 system required the insertion of an unconventional isopeptide bond (at the branching point), formed between the carboxyl terminus of G13′ and the amino group of the side chain of the branched K residue. For all three systems, PDB (protein data bank) files with the atomic coordinates and protein structure (PSF) files were generated with the PSFGEN plugin in VMD. Next, by using the Solvate plugin of VMD, the three protein systems were solvated in water boxes, which were preequilibrated under normal temperature ($T$ = 300 K) and pressure ($p$ = 1 atm). Each simulation box was sufficiently large to avoid self-interaction of the peptide with its own images during MD simulations under periodic boundary conditions. The final single copy, series, and parallel systems contained, respectively, a total of 10 350 (3373), 33 289 (10 914), and 58 109 (19 160) atoms (TIP3P water molecules). To mimic the physiological ionic strength of the solution used in the AFM experiments (300 mM), we used the Autoionize plugin in VMD and added a total of 19 (21), 109 (113), and 62 (67) $K^+$ ($Cl^-$) ions to the three systems. In each case, the extra anions were needed to neutralize the +2$e$ charge of SecA2-11.

*MD Simulations and Analysis.* To eliminate bad contacts, the SecA2-11 systems were energy minimized and then equilibrated for several tens of nanoseconds using the molecular dynamics program NAMD 2.9[51] with the CHARMM36 force field. The simulations were carried out under normal temperature and pressure. Periodic boundary conditions were used to reduce finite size effects. To mimic the experimental conditions, the alpha carbon ($C\alpha$) of the cysteine residue was harmonically restrained (spring constant $k$ = 7 kcal/mol/Å$^2$), as this end is connected to the PEG linker, which is in turn covalently affixed to the AFM tip. van der Waals interactions were truncated at



DOI: 10.1021/acs.langmuir.7b00100
Langmuir 2017, 33, 4057−4065

the cutoff distance of 12 Å with a smooth switching function starting at 10 Å. Long-range electrostatic interactions were computed using the particle mesh Ewald method[52] with a grid spacing of 1 Å. The MD equations of motion were integrated with a multiple time step algorithm: 1 fs for bonding interactions, 2 fs for nonbonding interactions, and 4 fs for electrostatic interactions. Constant temperature was maintained by coupling the system to a Langevin thermostat with a coupling coefficient of 1 $ps^{-1}$. The pressure was kept constant by using the Nosè−Hoover Langevin piston method[53] with a decay period of 100 fs and a damping timescale of 50 fs. Following equilibration (section S9), a 30 ns long MD production run was carried out for each system. The coordinates of all atoms were saved every 10 ps and subsequently used to study the conformational dynamics of the SecA2-11 peptides. The MD simulations were carried out on 48 Haswell cores with a performance of approximately 5 ns/day.

To quantify the degree of compactness of a single SecA2-11 peptide, we calculated the radius of gyration of the ($N$ = 10) C$\alpha$ atoms: $R_g = [\sum_i (r_i - r_c)^2/N]^{1/2}$, where $r_i$ is the position vector of the $i$th C$\alpha$ (at a given time) and $r_c$ is the corresponding centroid. The small standard deviations (<1 Å) of the radius of gyration for each SecA2-11 peptide imply that the systems were well-equilibrated. To quantify the relative orientation of the peptides in the series and parallel constructs, we calculated the time series of the angle $\theta$ between the axes of the SecA2-11s, defined as the principal axes of inertia of their C$\alpha$ atoms that correspond to the smallest principal moment of inertia.

## ■ ASSOCIATED CONTENT

### Supporting Information

The Supporting Information is available free of charge on the ACS Publications website at DOI: 10.1021/acs.langmuir.7b00100.

Incubation concentration study; control experiments using tips without peptides; lipid coating control experiment; polymerized lipid bilayer experiments with the parallel peptide; circular dichroism analysis; coupled high performance liquid chromatography and mass spectroscopy; AFM imaging verifies lipid bilayer coverage; force map analysis; and time evolution of the radius of gyration (PDF)

## ■ AUTHOR INFORMATION


### Corresponding Author

*E-mail: kinggm@missouri.edu.

### ORCID

Gavin M. King: 0000-0002-5811-7012


### Notes

The authors declare no competing financial interest.

## ■ ACKNOWLEDGMENTS

The authors gratefully acknowledge stimulating interactions with Linda L. Randall and all members of the Membrane Research Group at University of Missouri. We also thank Sonja Glaser, Thomas T. Perkins, Stephen H. White, and Martin B. Ulmschneider for discussions. This work was supported by the Burroughs Wellcome Fund (Career Award at the Scientific Interface), the National Science Foundation (CAREER Award #: 1054832), and the MU Research Board. The computation for this work was performed on the high performance computing infrastructure provided by Research Computing Support Services at the University of Missouri, Columbia MO.

## ■ REFERENCES


(1) Simon, S. A.; McIntosh, T. J. *Peptide−Lipid Interactions*; Academic Press, 2002; Vol. *52*.

(2) Phillips, R.; Ursell, T.; Wiggins, P.; Sens, P. Emerging roles for lipids in shaping membrane-protein function. *Nature* **2009**, *459*, 379−385.

(3) Cymer, F.; von Heijne, G.; White, S. H. Mechanisms of integral membrane protein insertion and folding. *J. Mol. Biol.* **2015**, *427*, 999−1022.

(4) Copolovici, D. M.; Langel, K.; Eriste, E.; Langel, Ü. Cell-penetrating peptides: Design, synthesis, and applications. *ACS Nano* **2014**, *8*, 1972−1994.

(5) Nguyen, L. T.; Haney, E. F.; Vogel, H. J. The expanding scope of antimicrobial peptide structures and their modes of action. *Trends Biotechnol.* **2011**, *29*, 464−472.

(6) White, S. H.; Wimley, W. C.; Ladokhin, A. S.; Hristova, K. Protein folding in membranes: Determining energetics of peptide-bilayer interactions. *Methods Enzymol.* **1998**, *295*, 62−87.

(7) Oesterhelt, F.; Oesterhelt, D.; Pfeiffer, M.; Engel, A.; Gaub, H. E.; Müller, D. J. Unfolding pathways of individual bacteriorhodopsins. *Science* **2000**, *288*, 143−146.

(8) Bippes, C. A.; Muller, D. J. High-resolution atomic force microscopy and spectroscopy of native membrane proteins. *Rep. Prog. Phys.* **2011**, *74*, 086601.

(9) Petrosyan, R.; Bippes, C. A.; Walheim, S.; Harder, D.; Fotiadis, D.; Schimmel, T.; Alsteens, D.; Müller, D. J. Single-molecule force spectroscopy of membrane proteins from membranes freely spanning across nanoscopic pores. *Nano Lett.* **2015**, *15*, 3624−3633.

(10) Rief, M.; Gautel, M.; Oesterhelt, F.; Fernandez, J. M.; Gaub, H. E. Reversible unfolding of individual titin immunoglobulin domains by AFM. *Science* **1997**, *276*, 1109−1112.

(11) Churnside, A. B.; Sullan, R. M. A.; Nguyen, D. M.; Case, S. O.; Bull, M. S.; King, G. M.; Perkins, T. T. Routine and timely sub-picoNewton force stability and precision for biological applications of atomic force microscopy. *Nano Lett.* **2012**, *12*, 3557−3561.

(12) Almquist, B. D.; Melosh, N. A. Fusion of biomimetic stealth probes into lipid bilayer cores. *Proc. Natl. Acad. Sci. U.S.A.* **2010**, *107*, 5815−5820.

(13) Min, D.; Jefferson, R. E.; Bowie, J. U.; Yoon, T.-Y. Mapping the energy landscape for second-stage folding of a single membrane protein. *Nat. Chem. Biol.* **2015**, *11*, 981−987.

(14) Desmeules, P.; Grandbois, M.; Bondarenko, V. A.; Yamazaki, A.; Salesse, C. Measurement of membrane binding between recoverin, a calcium-myristoyl switch protein, and lipid bilayers by AFM-based force spectroscopy. *Biophys. J.* **2002**, *82*, 3343−3350.

(15) Ganchev, D. N.; Rijkers, D. T. S.; Snel, M. M. E.; Killian, J. A.; de Kruijff, B. Strength of integration of transmembrane $\alpha$-helical peptides in lipid bilayers as determined by atomic force spectroscopy. *Biochemistry* **2004**, *43*, 14987−14993.

(16) Contera, S. A.; Lemaître, V.; de Planque, M. R. R.; Watts, A.; Ryan, J. F. Unfolding and extraction of a transmembrane $\alpha$-helical peptide: Dynamic force spectroscopy and molecular dynamics simulations. *Biophys. J.* **2005**, *89*, 3129−3140.

(17) Cross, B.; Ronzon, F.; Roux, B.; Rieu, J.-P. Measurement of the anchorage force between GPI-anchored alkaline phosphatase and supported membranes by AFM force spectroscopy. *Langmuir* **2005**, *21*, 5149−5153.

(18) Andre, G.; Brasseur, R.; Dufrêne, Y. F. Probing the interaction forces between hydrophobic peptides and supported lipid bilayers using AFM. *J. Mol. Recognit.* **2007**, *20*, 538−545.

(19) Takahashi, H.; Shahin, V.; Henderson, R. M.; Takeyasu, K.; Edwardson, J. M. Interaction of Synaptotagmin with Lipid Bilayers, Analyzed by Single-Molecule Force Spectroscopy. *Biophys. J.* **2010**, *99*, 2550−2558.

(20) Sun, S.; Zhao, G.; Huang, Y.; Cai, M.; Shan, Y.; Wang, H.; Chen, Y. Specificity and mechanism of action of alpha-helical membrane-active peptides interacting with model and biological membranes by single-molecule force spectroscopy. *Sci. Rep.* **2016**, *6*, 29145.




DOI: 10.1021/acs.langmuir.7b00100
*Langmuir* 2017, 33, 4057−4065

(21) Przybylo, M.; Sýkora, J.; Humpolíčková, J.; Benda, A.; Zan, A.; Hof, M. Lipid diffusion in giant unilamellar vesicles is more than 2 times faster than in supported phospholipid bilayers under identical conditions. *Langmuir* **2006**, *22*, 9096−9099.
(22) Sigdel, K. P.; Matin, T. R.; Chada, N.; Marsh, B. P.; King, C. R.; White, S. H.; Ulmschneider, M. B.; Kosztin, I.; King, G. M. The complex energy landscape of peptide−membrane interactions, submitted for publication, **2017**.
(23) Driessen, A. J. M.; Nouwen, N. Protein translocation across the bacterial cytoplasmic membrane. *Annu. Rev. Biochem.* **2008**, *77*, 643−667.
(24) Oliver, D. B.; Beckwith, J. Identification of a new gene (secA) and gene product involved in the secretion of envelope proteins in *Escherichia coli*. *J. Bacteriol.* **1982**, *150*, 686−691.
(25) Cabelli, R. J.; Dolan, K. M.; Qian, L. P.; Oliver, D. B. Characterization of membrane-associated and soluble states of SecA protein from wild-type and SecA51(TS) mutant strains of *Escherichia coli*. *J. Biol. Chem.* **1991**, *266*, 24420−24427.
(26) Chen, X.; Xu, H.; Tai, P. C. A significant fraction of functional SecA is permanently embedded in the membrane: SecA cycling on and off the membrane is not essential during protein translocation. *J. Biol. Chem.* **1996**, *271*, 29698−29706.
(27) Breukink, E.; Keller, R. C. A.; de Kruijff, B. Nucleotide and negatively charged lipid-dependent vesicle aggregation caused by SecA. Evidence that SecA contains two lipid-binding sites. *FEBS Lett.* **1993**, *331*, 19−24.
(28) Mori, H.; Sugiyama, H.; Yamanaka, M.; Sato, K.; Tagaya, M.; Mizushima, S. Amino-terminal region of SecA is involved in the function of SecG for protein translocation into *Escherichia coli* membrane vesicles. *J. Biochem.* **1998**, *124*, 122−129.
(29) Mao, C.; Cheadle, C. E.; Hardy, S. J. S.; Lilly, A. A.; Suo, Y.; Gari, R. R. S.; King, G. M.; Randall, L. L. Stoichiometry of SecYEG in the active translocase of *Escherichia coli* varies with precursor species. *Proc. Natl. Acad. Sci. U.S.A.* **2013**, *110*, 11815−11820.
(30) Bauer, B. W.; Shemesh, T.; Chen, Y.; Rapoport, T. A. A "push and slide" mechanism allows sequence-insensitive translocation of secretory proteins by the SecA ATPase. *Cell* **2014**, *157*, 1416−1429.
(31) Zimmermann, J. L.; Nicolaus, T.; Neuert, G.; Blank, K. Thiol-based, site-specific and covalent immobilization of biomolecules for single-molecule experiments. *Nat. Protoc.* **2010**, *5*, 975−985.
(32) Sackmann, E. Supported membranes: Scientific and practical applications. *Science* **1996**, *271*, 43−48.
(33) Richter, R. P.; Brisson, A. R. Following the formation of supported lipid bilayers on mica: A study combining AFM, QCM-D, and ellipsometry. *Biophys. J.* **2005**, *88*, 3422−3433.
(34) El Kirat, K.; Morandat, S.; Dufrêne, Y. F. Nanoscale analysis of supported lipid bilayers using atomic force microscopy. *Biochim. Biophys. Acta* **2010**, *1798*, 750−765.
(35) Cremer, P. S.; Boxer, S. G. Formation and Spreading of Lipid Bilayers on Planar Glass Supports. *J. Phys. Chem. B* **1999**, *103*, 2554.
(36) Chada, N.; Sigdel, K. P.; Gari, R. R. S.; Matin, T. R.; Randall, L. L.; King, G. M. Glass is a Viable Substrate for Precision Force Microscopy of Membrane Proteins. *Sci. Rep.* **2015**, *5*, 12550.
(37) Ainavarapu, S. R. K.; Brujić, J.; Huang, H. H.; Wiita, A. P.; Lu, H.; Li, L.; Walther, K. A.; Carrion-Vazquez, M.; Li, H.; Fernandez, J. M. Contour length and refolding rate of a small protein controlled by engineered disulfide bonds. *Biophys. J.* **2007**, *92*, 225−233.
(38) Farrance, O. E.; Paci, E.; Radford, S. E.; Brockwell, D. J. Extraction of accurate biomolecular parameters from single-molecule force spectroscopy experiments. *ACS Nano* **2015**, *9*, 1315−1324.
(39) Wieland, J. A.; Gewirth, A. A.; Leckband, D. E. Single-molecule measurements of the impact of lipid phase behavior on anchor strengths. *J. Phys. Chem. B* **2005**, *109*, 5985−5993.
(40) Stetter, F. W. S.; Cwiklik, L.; Jungwirth, P.; Hugel, T. Single lipid extraction: The anchoring strength of cholesterol in liquid-ordered and liquid-disordered phases. *Biophys. J.* **2014**, *107*, 1167−1175.
(41) Dudko, O.; Hummer, G.; Szabo, A. Intrinsic rates and activation free energies from single-molecule pulling experiments. *Phys. Rev. Lett.* **2006**, *96*, 108101.
(42) Dudko, O. K.; Hummer, G.; Szabo, A. Theory, analysis, and interpretation of single-molecule force spectroscopy experiments. *Proc. Natl. Acad. Sci. U.S.A.* **2008**, *105*, 15755−15760.
(43) Woodside, M. T.; Block, S. M. Reconstructing folding energy landscapes by single-molecule force spectroscopy. *Annu. Rev. Biophys.* **2014**, *43*, 19−39.
(44) Connolly, M. L. Solvent-accessible surfaces of proteins and nucleic acids. *Science* **1983**, *221*, 709−713.
(45) Kowalczyk, W.; Monsó, M.; de la Torre, B. G.; Andreu, D. Synthesis of multiple antigenic peptides (MAPs)-strategies and limitations. *J. Pept. Sci.* **2011**, *17*, 247−251.
(46) Hinterdorfer, P.; Baumgartner, W.; Gruber, H. J.; Schilcher, K.; Schindler, H. Detection and localization of individual antibody-antigen recognition events by atomic force microscopy. *Proc. Natl. Acad. Sci. U.S.A.* **1996**, *93*, 3477−3481.
(47) te Riet, J.; Katan, A. J.; Rankl, C.; Stahl, S. W.; van Buul, A. M.; Phang, I. Y.; Gomez-Casado, A.; Schön, P.; Gerritsen, J. W.; Cambi, A.; Rowan, A. E.; Vancso, G. J.; Jonkheijm, P.; Huskens, J.; Oosterkamp, T. H.; Gaub, H.; Hinterdorfer, P.; Figdor, C. G.; Speller, S. Interlaboratory round robin on cantilever calibration for AFM force spectroscopy. *Ultramicroscopy* **2011**, *111*, 1659.
(48) Sreerama, N.; Woody, R. W. Estimation of protein secondary structure from circular dichroism spectra: Comparison of CONTIN, SELCON, and CDSSTR methods with an expanded reference set. *Anal. Biochem.* **2000**, *287*, 252−260.
(49) Whitmore, L.; Wallace, B. A. Protein secondary structure analyses from circular dichroism spectroscopy: Methods and reference databases. *Biopolymers* **2008**, *89*, 392−400.
(50) Humphrey, W.; Dalke, A.; Schulten, K. VMD: Visual molecular dynamics. *J. Mol. Graphics* **1996**, *14*, 33−38.
(51) Phillips, J. C.; Braun, R.; Wang, W.; Gumbart, J.; Tajkhorshid, E.; Villa, E.; Chipot, C.; Skeel, R. D.; Kalé, L.; Schulten, K. Scalable molecular dynamics with NAMD. *J. Comput. Chem.* **2005**, *26*, 1781−1802.
(52) Darden, T.; York, D.; Pedersen, L. Particle mesh Ewald: An *N* log(*N*) method for Ewald sums in large systems. *J. Chem. Phys.* **1993**, *98*, 10089−10092.
(53) Martyna, G. J.; Tobias, D. J.; Klein, M. L. Constant pressure molecular dynamics algorithms. *J. Chem. Phys.* **1994**, *101*, 4177−4189.



DOI: 10.1021/acs.langmuir.7b00100
*Langmuir* 2017, 33, 4057−4065

# Supporting Information

# Single-molecule peptide-lipid affinity assay reveals interplay between solution structure and partitioning

**Tina R. Matin, Krishna P. Sigdel, Milica Utjesanovic, Brendan P. Marsh, Fabio Gallazzi, Virginia F. Smith, Ioan Kosztin, Gavin M. King***

***Electronic mail:** kinggm@missouri.edu

## 1) Optimizing tip functionalization

The number of peptides tethered to the vicinity of the tip apex is expected to scale with the concentration of peptides during the incubation step of the functionalization process.[1] Three incubation concentrations were evaluated in dissociation (Fig. S1):

1) **10 μM**: yield $Y = 10\%$, number of events ( ≥5 pN) $N_e = 75$, number of tips tested $N_t = 10$
2) **100 μM**: $Y = 50\%$, $N_e = 304$, $N_t = 10$
3) **1 mM**: $Y = 80\%$, $N_e = 407$, $N_t = 10$

Yield is defined as the number of active tips (i.e., tips which exhibit $N_e > 10$ rupture events) divided by the number of tips tested, expressed as a percentage. While the yield of the 1 mM incubation concentration was high, sub-populations at high rupture force (>50 pN) were observed. The presence of additional peaks in the force distribution at approximately twice the fundamental is suggestive of multiple tethers. In traces exhibiting >1 dissociation event (~20% for 100 μM), we plot only the last rupture. We note that the peak in the dissociation force histograms at approximately 20 pN was stable (+/- 1.4 pN) across the three concentrations studied and no stable lower force peaks were observed. We therefore take ~20 pN to represent the most probable rupture force for a single SecA2-11 molecule and POPC at this loading rate (~500 pN/s). Interestingly, the association force distributions (Fig. S1, inset) did not exhibit sub-populations, even when using 1 mM incubation concentration. We attribute this to stochastic peptide/lipid trajectories which do not favor simultaneous partitioning. 100 μM incubation concentration was employed for all constructs throughout this study as this concentration simultaneously minimizes the probability of multiple tethers while maintaining a significant yield (50%) of active tips.

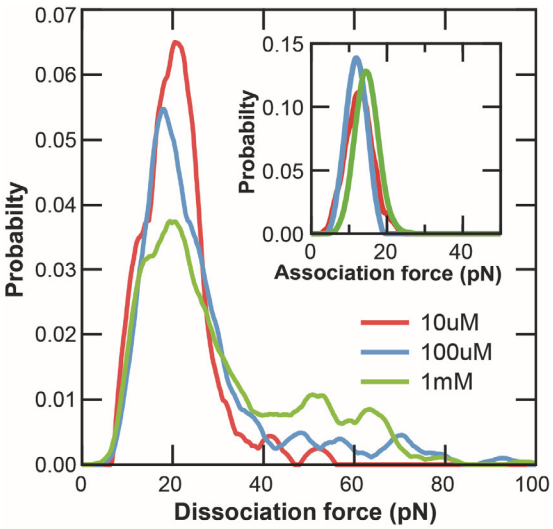


**Figure S1. Incubation concentration study.** Dissociation (rupture) force distributions for SecA2-11 single copy construct at three incubation concentrations: 10, 100, and 1000 μM. Inset: distribution of association events reveal similar single Gaussian-like distributions for the three incubation conditions. Note the horizontal scale is 2-fold expanded.

**2) Control experiments verify the source of the interaction**

In a first set of experiments (Fig. S2a), the interaction of 5 non-functionalized AFM tips ($N_t = 5$) with a bare glass substrate was monitored. Out of $N_a = 500$ attempts, $N_e = 3$ curves exhibited >5 pN of adhesion. In a second control (Fig. S2b), we used tips that contained all the components of the fully functionalized tips except with a cysteine termination instead of the peptide (i.e., NHS-PEG-maleimide-Cys) and a bare glass substrate. No evidence of adhesion was observed in this case ($N_e = 0$, $N_a = 500$, $N_t = 5$). We then mimicked the final experimental design without peptides on the tips. Specifically, we examined NHS-PEG-maleimide-Cys tips interacting with glass-supported POPC lipid bilayers (Fig. S2c). This produced $N_e = 13$ dissociation events >5 pN out of 500 attempts (activity, $A = 2.6\%$; $N_t = 5$). No association interactions >5 pN ($N_e = 0$, $A = 0\%$) were observed in the approach phase of the tip trajectory. The results imply that the great majority (>97%) of rupture events and all association events arise from specific peptide-lipid interactions.

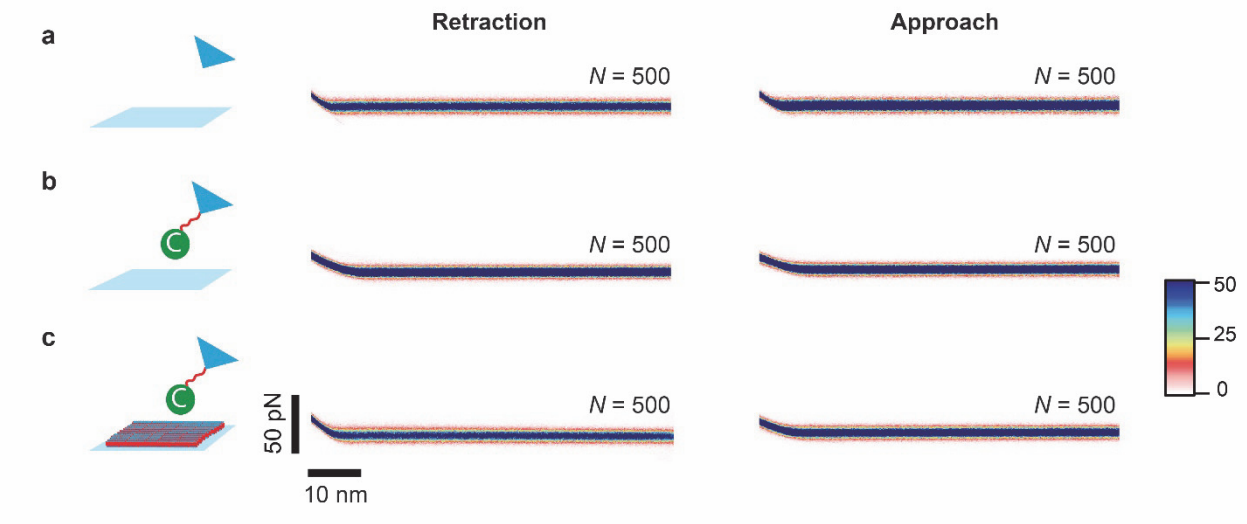


**Figure S2. Control experiments using tips without peptides.** Row (**a**) shows superimposed retraction and approach F-D curves with bare tips and bare glass. Row (**b**) displays data for NHS-PEG-maleimide-Cys functionalized tips and bare glass. Row (**c**) shows data for NHS-PEG-maleimide-Cys functionalized tips ($N_t = 5$) and glass-supported POPC bilayers.

### 3) Control experiments assess lipid adhesion on tip

As a further control, we tested the possibility of lipid coating over the peptide functionalized tips upon 'first touch' with the lipid bilayer, as has been reported using different peptide constructs.[2] In our experiments with SecA2-11, no long range repulsive interactions or changes of sign of the interaction were observed upon first contact with POPC. We demonstrate this by comparing the very first force curve with subsequent curves using the same identical SecA2-11 functionalized tip (Fig. S3). Based on the overlap observed between the first and subsequent traces, we ruled out lipid coating. We note that lipid coating upon 'first touch' is different than lipid pulling. Our observations suggest that the parallel SecA2-11 construct did (in ~40% of dissociation events) pull lipid (as discussed in Supplementary Information Section 4), but the lipid did not remain adhered to the tip in subsequent force curves.

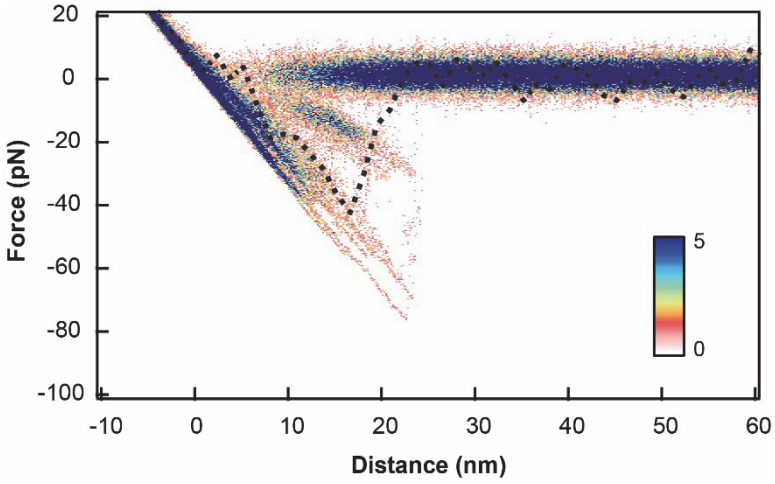


**Figure S3. Lipid coating control experiment.** The very first retraction interaction (dotted black line) between a new, freshly functionalized SecA2-11 single copy tip and a POPC bilayer is overlaid on a density plot of all subsequent curves recorded with the same identical tip ($A$ = 93%, $N_e$ = 100). No significant differences between the first and subsequent traces were observed.

**4) Control experiments with UV-crosslinked lipids and the parallel peptide construct**

We hypothesized that in some cases the SecA2-11 parallel construct was pulling POPC molecules from the underlying glass surface. To assess this, we utilized photo-polymerizable lipids [1,2-bis(10,12-tricosadiynoyl)-sn-glycero-3-phosphocholine (DC8,9PC), Avanti Polar Lipids] with tail groups that crosslink upon UV-exposure. Prior to force spectroscopy experiments, lipids were suspended in 50 mM sodium phosphate pH 7.2, 50 mM NaCl, 10 mM ethylenediaminetetraacetic acid (EDTA) and prepared via sonication. Liposomes went through 3 cycles of 30 min sonication at 55 °C in an ultrasonic bath (Branson 5510R-MTH) and stirring at room temperature for 15 min until the solution was clear.[3] Vesicles were deposited onto cleaned glass coverslips[4] to form supported lipid bilayers.[5] To minimize the probability of crosslinking during processing, all steps prior to UV-irradiation were carried out under yellow light (~600 nm). Glass substrates carrying the supported lipid bilayer were cooled (~ 0°C) prior to and during UV-irradiation in order to optimize the polymerization process.[6,7] Supported lipid bilayers were exposed to UV irradiation (UVGL-25 Compact UV Lamp, 254/365 nm, 4W) for 30 minutes keeping the UV lamp at a distance of approximately 3 cm.[8] Substrates were stored in a water saturated environment at room temperature prior to use. The resulting force spectroscopy data (Fig. S4) exhibited a significant reduction in the population of the high force tail (>50 pN) compared to standard POPC lipids. We note that the force required to extract an individual lipid molecule from a bilayer has been measured experimentally and simulated via molecular dynamics.[9] The force magnitude depends on a number of factors including the lipid species, phase of the bilayer (temperature), and loading rate. In conditions similar to ours, careful studies performed in the Leckband laboratory [10] revealed an average rupture force of 59 ± 11 pN to extract individual DMPC molecules from a fluid phase DMPC bilayer (1500 pN/s loading rate). Note that this value is significantly (>2-fold) above the prominent dissociation force that we measured for the SecA2-11 single copy construct (~19 pN, 550 pN/s loading rate), even after adjusting for loading rate differences.

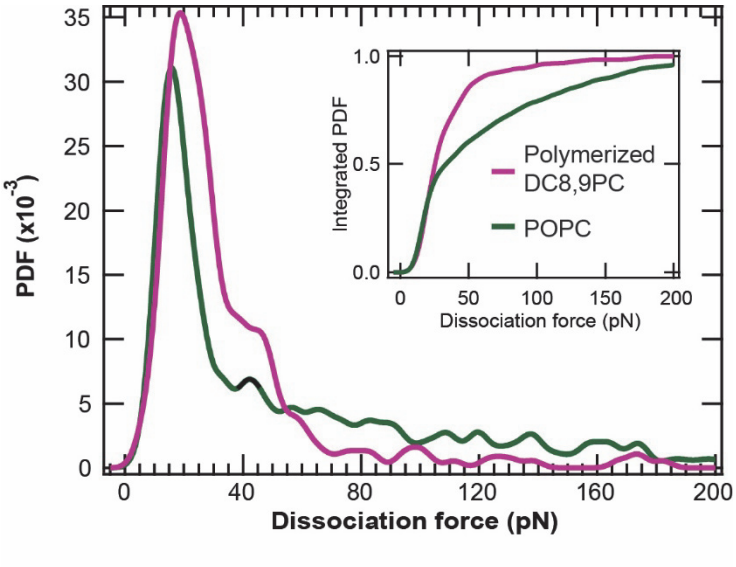


**Figure S4. Polymerized lipid bilayer experiments with the parallel peptide.** Probability density distribution of rupture events for parallel SecA2-11 using photo-polymerized1,2-bis(10,12-tricosadiynoyl)-sn-glycero-3-phosphocholine (DC8,9PC) lipids (*purple*; $A$ = 36%, $N_e$ = 701, $N_t$ = 8). For reference, data using standard POPC is overlaid (*green*; $A$ = 85%, $N_e$ = 667, $N_t$ = 8). Inset: integrated probability densities.

**5) Macroscopic measurements assess peptide secondary structure**

Circular dichroism spectroscopy (Fig. S5, see Materials and Methods for details) was performed to evaluate the secondary structural content of the single copy SecA2-11 peptide in solution and in contact with POPC lipid. The alpha-helical content remained low (<16 %) across all lipid concentrations tested, whereas, a high percentage (>50%) of disordered and turn structures were observed in all conditions.

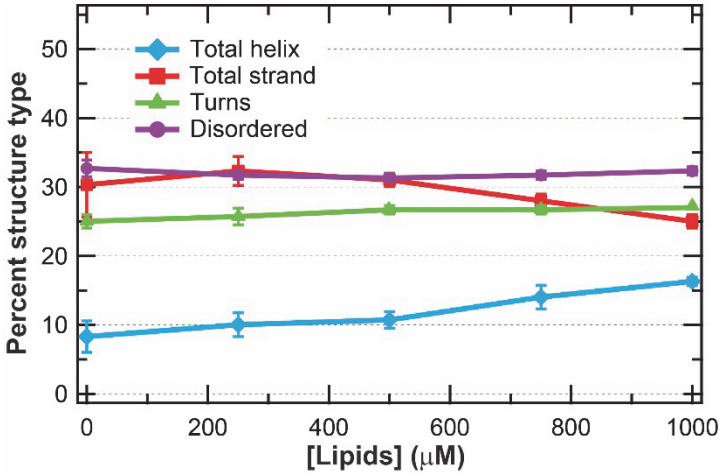


**Figure S5. Circular dichroism analysis.** Distribution of secondary structural elements plotted for single copy SecA2-11 titrated with POPC liposomes.

## 6) Mass Spectroscopy data for the three peptide constructs

### a) Single Copy SecA2-11

Calc MW: 1233.7 Da (MH$^+$ and MH$_2^{++}$ shown)

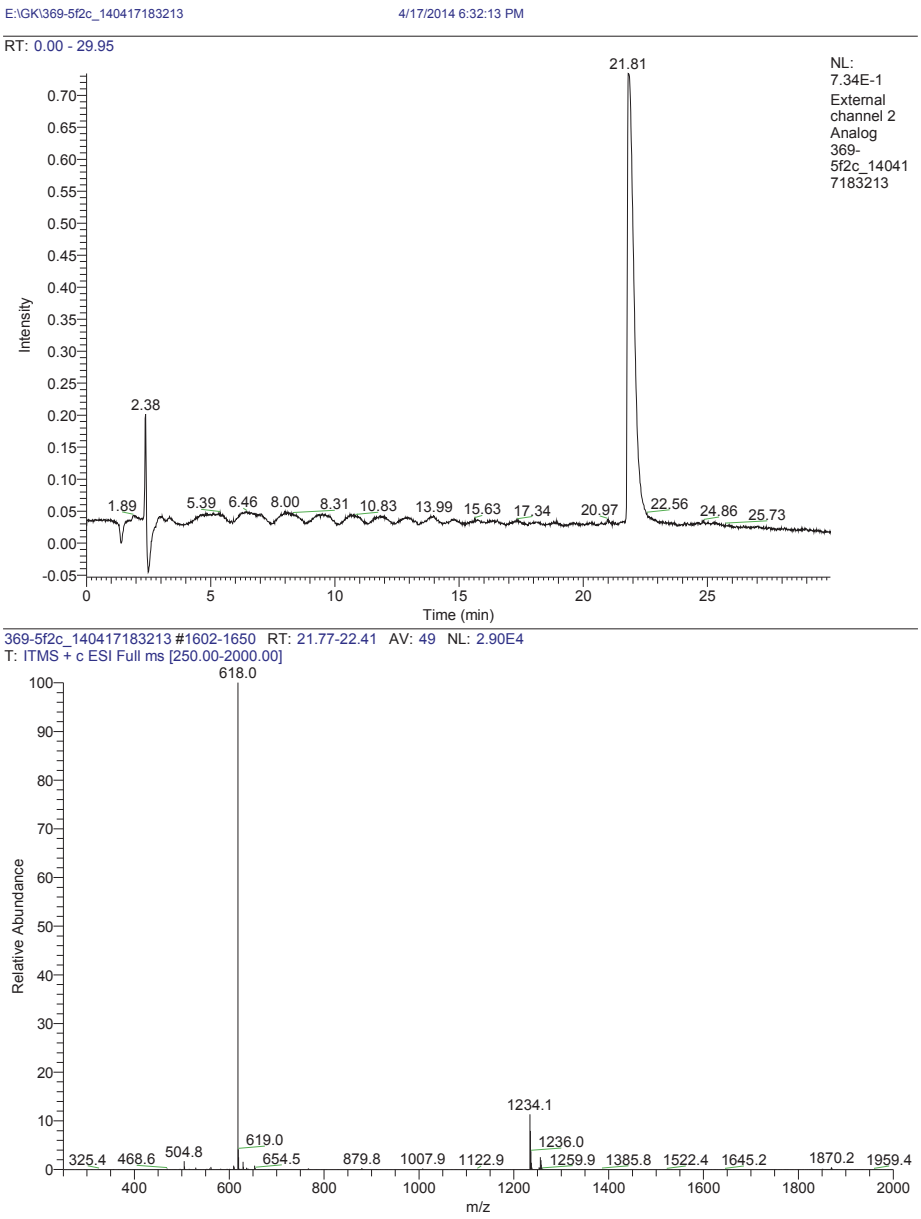

## b) SecA2-11 Parallel

Calculated MW: 2701.7 Da ($MNa^{+}$ , $MH_2^{++}$ ,$MH_3^{+++}$ and $MH_4^{++++}$ shown)

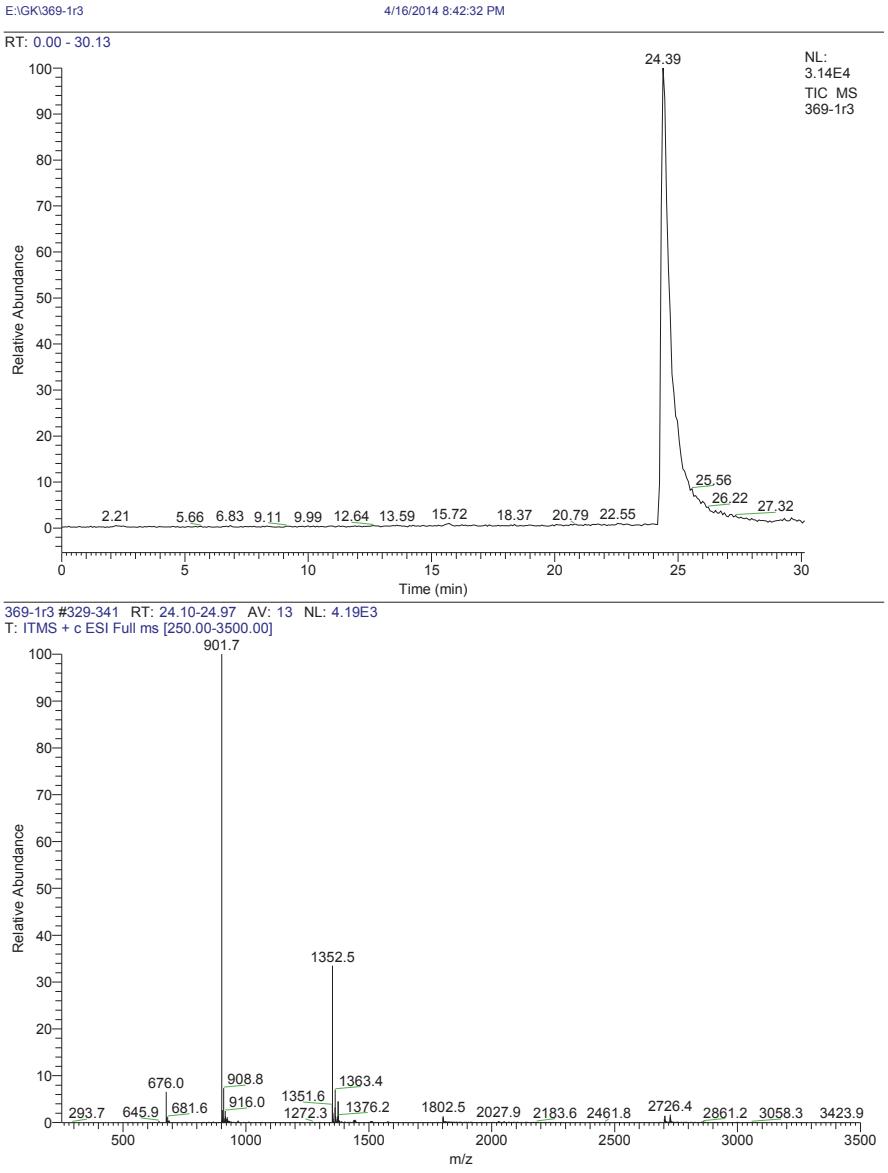

**c) SecA2-11 Series**

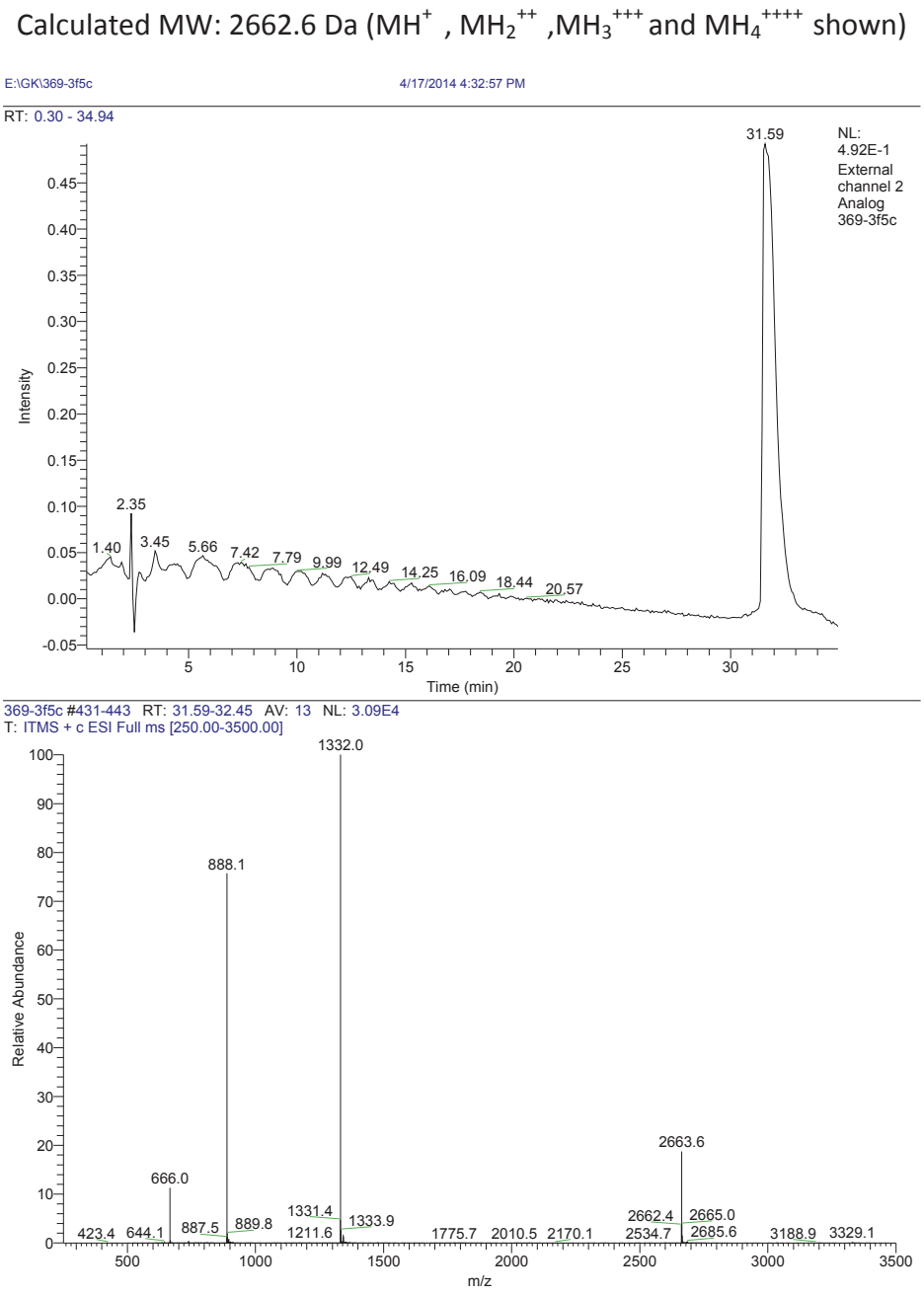


**Figure S6. Coupled high performance liquid chromatography and mass spectroscopy.** Time series and mass data is shown for the three synthetic peptide constructs: (**a**) single copy SecA2-11, (**b**) parallel SecA2-11, and (**c**) series SecA2-11.

**7) AFM imaging confirms lipid bilayer coverage**

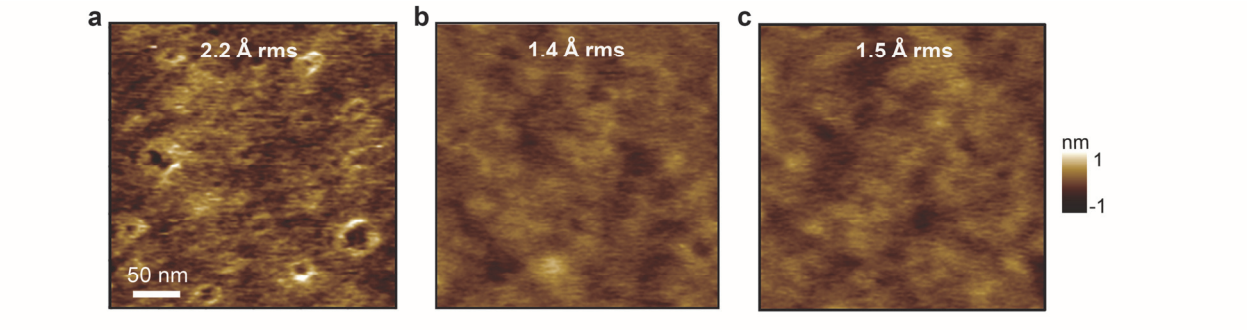


**Figure S7. AFM imaging verifies lipid bilayer coverage.** Lipid vesicles with zwitterionic head groups such as POPC are known to fuse rapidly and robustly onto clean glass surfaces over a wide range of solution conditions, forming supported lipid bilayers over large areas.[4,11,12] Following previous work, we confirmed vesicle fusion by analyzing surface roughness. Comparison of image data acquired (**a**) before and (**b**, **c**) after incubation with POPC vesicles (70 μM, 30 min) shows a significant reduction in roughness (from 2.2 to ~1.5 Å rms, calculated over 90,000 $nm^2$). This effective smoothening of the surface is indicative of a continuous bilayer coating,[4] and does not degrade over the timescale of the force spectroscopy experiments (**c** acquired 120 min after **b**). We note that the same identical AFM tip, imaging conditions, and analysis method was used for all images (tapping mode, Olympus Biolever mini tip, 1.9 nm/pixel, in buffer: 75 mM $Na_3PO_4$, pH 7.2, surfaces were rinsed with buffer (0.1 mL, 3x) prior to imaging, image data 1$^{st}$ order flattened).

**8) Force maps reveal similar tip-sample interactions over multiple length scales**

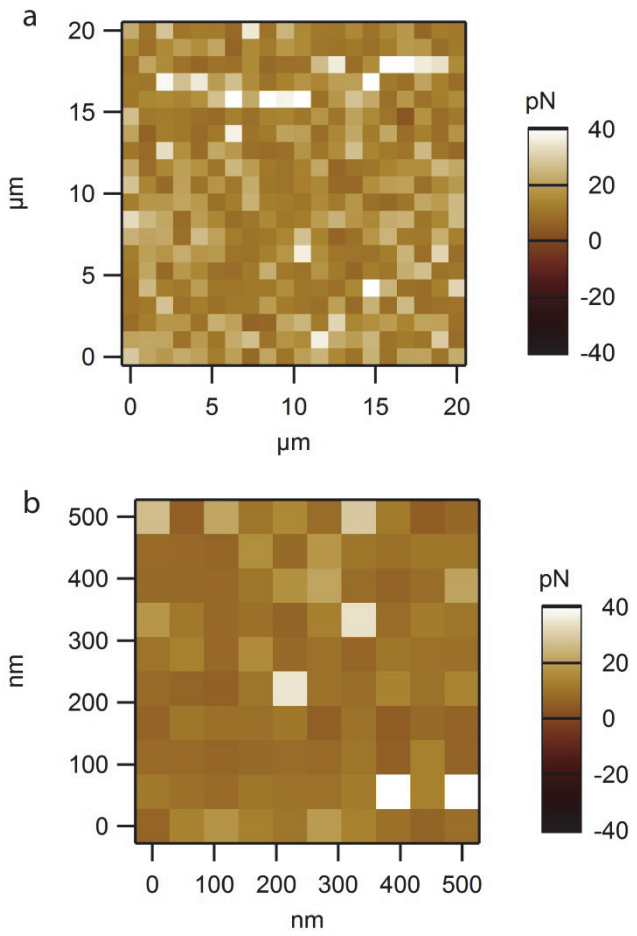


**Figure S8. Force map analysis.** (**a**) Distribution of tip-sample rupture force magnitude for a SecA2-11 single copy tip and a POPC bilayer over a 400 $\mu m^2$ area. Data acquired over a smaller area (0.25 $\mu m^2$) exhibited a similar stochastic distribution of rupture forces (**b**). The cantilever spring constant and pulling speed was ~6 pN/nm and 100 nm/s for both data sets.

**9) Radius of gyration, $R_g$, of the individual SecA2-11 monomers (with sub-Angstrom standard deviation) in all three constructs throughout the 30ns MD production run indicate that the systems were well equilibrated**

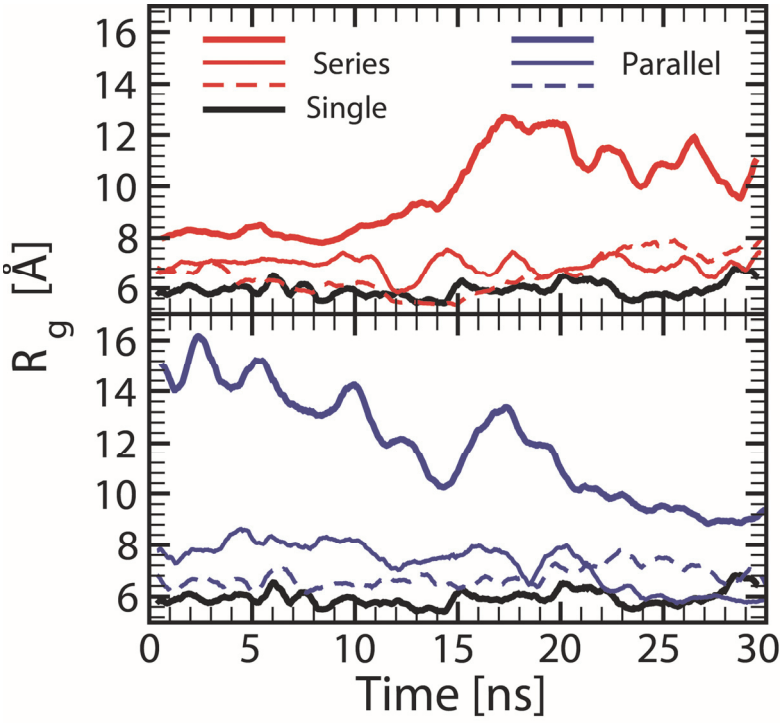


**Figure S9. Time evolution of the radius of gyration.** The radius of gyration ($R_g$) of the Cα atoms of SecA2-11 in the series (top panel, red) and parallel (bottom panel, blue) constructs plotted versus time. Thin-solid and thin dashed curves correspond to the two SecA2-11 monomers in the series (red) and parallel (blue) systems, and show similar behavior to $R_g$ for the single copy system (black, shown in both panels). In contrast, $R_g$ for the entire series (parallel) construct, shown as thick-solid red (blue) curve, exhibits significant variation in time, indicative of noticeable conformational changes as described in the manuscript.

## References cited:


1 Zimmermann, J. L., Nicolaus, T., Neuert, G. & Blank, K. Thiol-based, site-specific and covalent immobilization of biomolecules for single-molecule experiments. *Nat Protoc* **5**, 975-985 (2010).

2 Andre, G., Brasseur, R. & Dufrene, Y. F. Probing the interaction forces between hydrophobic peptides and supported lipid bilayers using AFM. *Journal of molecular recognition : JMR* **20**, 538-545, doi:10.1002/jmr.837 (2007).

3 Pei, L. & Lucy, C. A. Polymerized phospholipid bilayers as permanent coatings for small amine separations using mixed aqueous/organic capillary zone electrophoresis. *J Chromatogr A* **1267**, 80-88, doi:10.1016/j.chroma.2012.07.017 (2012).

4 Chada, N. *et al.* Glass is a Viable Substrate for Precision Force Microscopy of Membrane Proteins. *Sci Rep* **5**, 12550, doi:10.1038/srep12550 (2015).

5 Cremer, P. S. & Boxer, S. G. Formation and Spreading of Lipid Bilayers on Planar Glass Supports. *The Journal of Physical Chemistry B* **103**, 2554-2559, doi:10.1021/jp983996x (1999).

6 Muller, D. J. *et al.* Stability of bacteriorhodopsin alpha-helices and loops analyzed by single-molecule force spectroscopy. *Biophysical journal* **83**, 3578-3588, doi:10.1016/s0006-3495(02)75358-7 (2002).

7 Lopez, E., O'Brien, D. F. & Whitesides, T. H. Effects of membrane composition and lipid structure on the photopolymerization of lipid diacetylenes in bilayer membranes. *Biochimica et Biophysica Acta (BBA) - Biomembranes* **693**, 437-443, doi:http://dx.doi.org/10.1016/0005-2736(82)90451-5 (1982).

8 Okazaki, T. *et al.* Polymerized lipid bilayers on a solid substrate: morphologies and obstruction of lateral diffusion. *Langmuir : the ACS journal of surfaces and colloids* **25**, 345-351, doi:10.1021/la802670t (2009).

9 Stetter, F. W., Cwiklik, L., Jungwirth, P. & Hugel, T. Single lipid extraction: the anchoring strength of cholesterol in liquid-ordered and liquid-disordered phases. *Biophysical journal* **107**, 1167-1175, doi:10.1016/j.bpj.2014.07.018 (2014).

10 Wieland, J. A., Gewirth, A. A. & Leckband, D. E. Single-molecule measurements of the impact of lipid phase behavior on anchor strengths. *J Phys Chem B* **109**, 5985-5993, doi:10.1021/jp045461b (2005).

11 Andrecka, J., Spillane, K. M., Ortega-Arroyo, J. & Kukura, P. Direct observation and control of supported lipid bilayer formation with interferometric scattering microscopy. *ACS nano* **7**, 10662-10670, doi:10.1021/nn403367c (2013).

12 Cremer, P. S. & Boxer, S. G. Formation and Spreading of Lipid Bilayers on Planar Glass Supports. *J. Phys. Chem. B* **103**, 2554 (1999).